

Modelling the cosmic neutral hydrogen from DLAs and 21 cm observations

Hamsa Padmanabhan^{1*}, T. Roy Choudhury^{2†}, Alexandre Refregier^{3‡}

¹ *Inter-University Centre for Astronomy and Astrophysics, Pune 411007, India*

² *National Centre for Radio Astrophysics, Tata Institute of Fundamental Research, Pune 411007, India*

³ *Institute for Astronomy, Eidgenössische Technische Hochschule Zurich, Wolfgang-Pauli-Strasse 27, CH-8093 Zürich, Switzerland*

ABSTRACT

We review the analytical prescriptions in the literature to model the 21-cm (emission line surveys/intensity mapping experiments) and Damped Lyman-Alpha (DLA) observations of neutral hydrogen (HI) in the post-reionization universe. While these two sets of prescriptions have typically been applied separately for the two probes, we attempt to connect these approaches to explore the consequences for the distribution and evolution of HI across redshifts. We find that a physically motivated, 21-cm based prescription, extended to account for the DLA observables provides a good fit to the majority of the available data, but cannot accommodate the recent measurement of the clustering of DLAs at $z \sim 2.3$. This highlights a tension between the DLA bias and the 21-cm measurements, unless there is a very significant change in the nature of HI-bearing systems across redshifts 0-3. We discuss the implications of our findings for the characteristic host halo masses of the DLAs and the power spectrum of 21-cm intensity fluctuations.

Key words: cosmology:theory - cosmology:observations - large-scale structure of the universe - radio lines : galaxies.

1 INTRODUCTION

Understanding the distribution and evolution of neutral hydrogen in the universe provides key insights into cosmology, galaxy formation and the epoch of cosmic reionization. Two independent observational techniques are used to determine the abundance of neutral hydrogen at low and intermediate redshifts in the post-reionization universe. At low redshifts ($z \sim 0 - 1$), the neutral hydrogen density distribution is studied through observations of the redshifted 21-cm emission line at radio wavelengths. 21-cm emission line surveys provide three-dimensional maps of the density and velocity fields and thus offer a tomographic probe of the universe. Several galaxy surveys (Barnes et al. 2001; Meyer et al. 2004; Zwaan et al. 2005a; Lang et al. 2003; Jaffé et al. 2012; Rhee et al. 2013; Giovanelli et al. 2005; Martin et al. 2010; Catinella et al. 2010; Lah et al. 2007, 2009) as well as intensity mapping experiments (without resolving individual clumps of galaxies, e.g. Chang et al. (2010); Masui et al. (2013); Switzer et al. (2013)) provide constraints on the neutral hydrogen density (Ω_{HI}) and bias (b_{HI}) parameter at low redshifts. A compilation of the currently available constraints on the neutral hydrogen density and bias parameter, and the implications for intensity mapping experiments, has been recently provided in Padmanabhan, Choudhury & Refregier (2015)

(hereafter Paper I). The inherent weakness of the 21-cm line transition and the limits of current radio facilities, however, hamper the detection of HI in emission at higher redshifts ($z \gtrsim 2$). Upcoming surveys, which aim to detect this weak signal at intermediate and high redshifts, include those with the the Giant Meterwave Radio Telescope (Swarup et al. 1991, GMRT), the Meer-Karoo Array Telescope (Jonas 2009, MeerKAT), the Square Kilometre Array (SKA),¹ and the Canadian Hydrogen Intensity Mapping Experiment (CHIME)², among others.

At higher redshifts, our current understanding of the distribution of HI comes from the observations of Damped Lyman-Alpha systems (DLAs). DLAs are Lyman- α absorption systems which have column densities $N_{\text{HI}} \gtrsim 10^{20} \text{ cm}^{-2}$, and hence are self-shielded against the background ionizing radiation. Between the redshifts of 2 and ~ 5 , the majority of neutral hydrogen in the universe is thought to reside in DLAs (Wolfe et al. 1986; Lanzetta et al. 1991; Storrie-Lombardi & Wolfe 2000; Gardner et al. 1997; Prochaska, Herbert-Fort & Wolfe 2005). DLAs are also believed to be the primary reservoirs of neutral gas for the formation of stars and galaxies at lower redshifts, and hence the progenitors of today’s star-forming galaxies. Studies of DLAs have primarily focussed on the Lyman- α absorption lines of hydrogen in the spectra of high-redshift quasars (Noterdaeme et al. 2009,

* Electronic address: hamsa@iucaa.ernet.in

† Electronic address: tirth@ncra.tifr.res.in

‡ Electronic address: alexandre.refregier@phys.ethz.ch

¹ <https://www.skatelescope.org>

² <http://chime.phas.ubc.ca>

2012; Prochaska & Wolfe 2009; Prochaska, Herbert-Fort & Wolfe 2005; Zafar et al. 2013). A challenge in understanding the nature of DLAs is the identification of the host galaxies of the absorbers, the host halo masses and their properties. Imaging surveys for DLAs include those from Fynbo et al. (2010, 2011, 2013); Bouché et al. (2013); Rafelski et al. (2014); Fumagalli et al. (2014), many of which point to evidence for DLAs arising in the vicinity of faint, low star-forming galaxies. Unfortunately, the presence of the bright background QSO makes the direct imaging of DLAs difficult, and thus inhibits the identification of host galaxies situated at low impact parameters. With large sample sizes available in current data (e.g., Fumagalli et al. 2014), this caveat has lessened considerably, however, the precise understanding of the nature of DLAs still remains controversial.

On the theoretical front, a number of numerical simulations as well as analytical models have focussed on reproducing the observed HI content in galaxies and DLAs (Bagla, Khandai & Datta 2010; Nagamine et al. 2007; Pontzen et al. 2008; Tesfari et al. 2009; Hong et al. 2010; Cen 2012; Bird et al. 2014; Davé et al. 2013; Barnes & Haehnelt 2009, 2010, 2014). Numerical methods typically involve hydrodynamical simulations with detailed modelling of star formation, feedback, self-shielding and galactic outflows. These are then compared to the available observations of Ω_{HI} and b_{HI} , and the DLA observables such as the metallicity, bias, column density distribution and velocity widths. The free parameters in the physical processes involved are thus constrained by the observational data.

Analytical approaches (Bagla, Khandai & Datta 2010; Barnes & Haehnelt 2009, 2010, 2014) use prescriptions for assigning HI gas to dark matter haloes of different masses, and derive various quantities related to the 21-cm and DLA based observations. The DLA based models typically assume a physically motivated form for the HI distribution profile (Barnes & Haehnelt 2010, 2014) and/or the cross section of DLAs (Barnes & Haehnelt 2009) and fix the model free parameters by fitting to the available observations. Apart from being computationally less intensive, these approaches allow direct physical interpretation of the various quantities related to the HI distribution, and their evolution across redshifts. The prescriptions thus proposed are also used together with the results of N-body (Guha Sarkar et al. 2012) or smoothed-particle hydrodynamics (SPH) simulations (Villaescusa-Navarro et al. 2014) to study the distribution of post-reionization HI. The quantities of interest in the modelling of DLAs and 21-cm observations are thus dependent upon the prescriptions for assigning HI gas to dark matter host haloes of various masses. These, in turn, are connected to the properties of the DLA hosts and the nature of the DLAs themselves.

The 21-cm and DLA-based observations are thus independently associated with their corresponding analytical techniques in the literature. Here, we attempt to take into account all the available data in a common framework from both these sets of observations. We begin by reviewing the basic features of the 21-cm and the DLA based analytical techniques in the literature. We then summarize the latest available observational data from the 21-cm and DLA-based measurements. We explore the possibility of fitting all the available data with the analytical models across redshifts, and fix the model free parameters by comparing it to the observations. Once the free parameters are fixed, the remaining observables arise as predictions of the model and can be compared directly to the data. We discuss the implications of our findings for the DLA host halo masses, and the power spectrum of 21-cm intensity fluctuations

to be observed in current and future experiments (e.g., Bull et al. 2015; Santos et al. 2015).

Throughout the analysis, we use the cosmological parameters $\Omega_{\Lambda} = 0.719$, $\Omega_m = 0.281$, $\Omega_b = 0.0462$, $h = 0.71$, $\sigma_8 = 0.8$, $n_s = 0.963$ which are in good agreement with most available observations, including the latest Planck results (Planck Collaboration et al. 2013). The helium fraction by mass is taken to be $Y_p = 0.24$ (Olive & Skillman 2004).

2 THEORY

In the present section, we briefly review the theoretical approaches towards modelling the observations of DLAs and neutral hydrogen intensity mapping experiments.

2.1 21-cm based prescriptions

The two quantities of interest associated with the neutral hydrogen intensity mapping experiments (i.e. without resolving individual galaxies) are (a) the neutral hydrogen density parameter, Ω_{HI} and (b) the bias parameter b_{HI} . To model these properties, either analytically or through N -body simulations, a dark matter halo mass function $n(M, z)$ is assumed, following e.g. the Sheth-Tormen halo mass function (Sheth & Tormen 2002). A prescription $M_{\text{HI}}(M, z)$ is used to assign HI gas (of mass M_{HI}) to the halo (of mass M). The neutral hydrogen density parameter Ω_{HI} is then defined from the prescription as:

$$\Omega_{\text{HI}}(z) = \frac{1}{\rho_{c,0}} \int_0^{\infty} n(M, z) M_{\text{HI}}(M, z) dM \quad (1)$$

where $n(M, z)$ denotes the distribution of the dark matter halos and $\rho_{c,0}$ is the critical density of the universe at redshift 0. Given the prescription for $M_{\text{HI}}(M, z)$, the HI bias may be calculated as:

$$b_{\text{HI}}(z) = \frac{\int_0^{\infty} dM n(M, z) b(M, z) M_{\text{HI}}(M, z)}{\int_0^{\infty} dM n(M, z) M_{\text{HI}}(M, z)} \quad (2)$$

where the dark matter halo bias $b(M, z)$ is given, for example, following Scoccimarro et al. (2001).

In surveys of 21-cm emission from galaxies, the lower limits in the integrals in Eq. (2) are fixed to the halo mass M_{min} corresponding to the minimum HI mass observable by the survey. This leads to the expression for the HI bias measured from galaxy surveys³:

$$b_{\text{HI,gal}}(z) = \frac{\int_{M_{\text{min}}}^{\infty} dM n(M, z) b(M, z) M_{\text{HI}}(M, z)}{\int_{M_{\text{min}}}^{\infty} dM n(M, z) M_{\text{HI}}(M, z)} \quad (3)$$

2.2 DLA based prescriptions

In the case of Damped Lyman Alpha system (DLAs) observations, the primary observable is the distribution function of neutral hydrogen in DLAs, i.e. $f_{\text{HI}}(N_{\text{HI}})$ where N_{HI} is the column density of the DLAs. From the observations of $f_{\text{HI}}(N_{\text{HI}})$, the density parameter of neutral hydrogen in DLAs, Ω_{DLA} and dN/dX , the incidence rate of the DLAs per unit comoving absorption path length, may be inferred. Recently, the bias parameter of DLAs, b_{DLA} has been

³ Eq. (3) makes the approximation that the selection function of the HI galaxies can be modelled by a combination of HI mass weighting and a low-mass cutoff.

estimated at redshift $z \sim 2.3$ by cross-correlation studies with the Lyman- α forest (Font-Ribera et al. 2012). To explain the measured values of these observables, the DLA may be modelled as an absorbing cloud in a host dark matter halo of mass M , with a neutral hydrogen density profile $\rho_{\text{HI}}(r)$ as a function of r .

The column density of DLAs is then calculated using the relation:

$$N_{\text{HI}}(s) = \frac{2}{m_H} \int_0^{\sqrt{R_v(M)^2 - s^2}} \rho_{\text{HI}}(r = \sqrt{s^2 + l^2}) dl \quad (4)$$

where m_H is the mass of the hydrogen atom, $R_v(M)$ is the virial radius associated with a halo of mass M and s is the impact parameter of a line-of-sight through the DLA. The cross-section σ_{DLA} is defined as $\sigma_{\text{DLA}} = \pi s_*^2$ where s_* is the root of the equation $N_{\text{HI}}(s_*) = 10^{20.3} \text{ cm}^{-2}$. The DLA bias b_{DLA} is defined by:

$$b_{\text{DLA}}(z) = \frac{\int_0^\infty dM n(M, z) b(M, z) \sigma_{\text{DLA}}(M, z)}{\int_0^\infty dM n(M, z) \sigma_{\text{DLA}}(M, z)}. \quad (5)$$

The incidence dN/dX is calculated as:

$$\frac{dN}{dX} = \frac{c}{H_0} \int_0^\infty n(M, z) \sigma_{\text{DLA}}(M, z) dM \quad (6)$$

The column density distribution $f_{\text{HI}}(N_{\text{HI}}, z)$ is given by:

$$f(N_{\text{HI}}, z) = \frac{c}{H_0} \int_0^\infty n(M, z) \left| \frac{d\sigma}{dN_{\text{HI}}}(M, z) \right| dM \quad (7)$$

where the $d\sigma/dN_{\text{HI}} = 2\pi s ds/dN_{\text{HI}}$, with $N_{\text{HI}}(s)$ defined as in Eq. (4).

Finally, the density parameter for DLAs, Ω_{DLA} is calculated as:

$$\Omega_{\text{DLA}}(N_{\text{HI}}, z) = \frac{m_H H_0}{c \rho_{c,0}} \int_{10^{20.3}}^\infty f_{\text{HI}}(N_{\text{HI}}, z) N_{\text{HI}} dN_{\text{HI}} \quad (8)$$

Alternatively, the cross section $\sigma_{\text{DLA}}(M)$ itself is modelled using a functional form, and the DLA quantities may be directly calculated from σ_{DLA} .

3 DATA

In the present section, we compile the currently available constraints from the 21-cm and DLA observations (a detailed summary is available in Paper I):

(a) Constraints on Ω_{HI} from 21-cm galaxy surveys include those from Delhaize et al. (2013, HIPASS and the Parkes observations of the SGP field at $z \sim 0.03$ and 0.1), Rhee et al. (2013, WSRT 21-cm emission at $z = 0.1$ and 0.2), Martin et al. (2010, ALFALFA survey observations), Freudling et al. (2011, AUDES survey at $z \sim 0.125$), and Lah et al. (2007, co-added observations from the GMRT at $z = 0.24$).

(b) Joint constraints on the product $\Omega_{\text{HI}} b_{\text{HI}}$ from 21-cm intensity mapping experiments at $z \sim 0.8$ come from Chang et al. (2010), Masui et al. (2013) and Switzer et al. (2013).

(c) Constraints on the neutral mass fraction in DLAs, Ω_{DLA} at $z \sim 0$ are available from Braun (2012, observations of HI distribution in M31, M33 and the Large Magellanic Cloud (LMC)), Zwaan et al. (2005a, HIPASS catalogue, $z \sim 0$), and at $0.5 < z < 5$ from the observations of Rao, Turnshek & Nestor (2006), Prochaska & Wolfe (2009), Noterdaeme et al. (2009), Noterdaeme et al. (2012) and Zafar et al. (2013).

(d) Constraints on the bias parameter b_{HI} at $z \sim 0$ are available from the ALFALFA survey (Martin et al. 2012).

(e) Constraints on the DLA incidence dN/dX at $z \sim 0$ are available from Braun (2012), Zwaan et al. (2005b), and at $z \sim 1$ from Rao, Turnshek & Nestor (2006). Zafar et al. (2013) compiles the currently available constraints on the DLA incidence dN/dX over $1.5 < z < 4$.

(f) The HI column density distribution f_{HI} at redshift $z \sim 2.5$ comes from the observations of Noterdaeme et al. (2012). The column density distribution at redshift $z \sim 0$ is available from the observations of Zwaan et al. (2005b) and at $z \sim 1$ from Rao, Turnshek & Nestor (2006).

(g) Font-Ribera et al. (2012) provide a measurement of the bias parameter b_{DLA} of DLAs at redshift $z \sim 2.3$.

4 MODELS

We now attempt to model the neutral hydrogen distribution by considering both DLAs and 21-cm intensity mapping measurements. To begin with, we describe some of the models available in the literature to assign HI to dark matter haloes and compute the relevant quantities in the 21-cm and DLA based prescriptions.

(i) 21-cm based: Bagla, Khandai & Datta (2010) explore several prescriptions for assigning HI gas to dark matter haloes to be used with the results of N-body simulations. In their simplest model, $M_{\text{HI}}(M)$ is modelled as $M_{\text{HI}} = fM$ between limits M_{min} and M_{max} that correspond to virial velocities of 30 km/s and 200 km/s respectively. The value of f is chosen to match the observations of Ω_{HI} .

(ii) DLA based: Barnes & Haehnelt (2009, 2010) develop analytical models to explain various observed properties of the DLAs at $z \sim 3$, such as their column density distribution and velocity width distribution. Barnes & Haehnelt (2014) jointly model the column density distribution, the velocity width distribution of associated low-ionization metal absorption and the observed bias parameter of DLAs at $z \sim 2.3$.

In Barnes & Haehnelt (2009), the cross-section $\sigma_{\text{DLA}}(M)$ is modelled using the functional form:

$$\sigma_{\text{DLA}}(M) = \pi r_0^2 \left(\frac{v_c}{200 \text{ km/s}} \right)^\beta \exp \left[- \left(\frac{v_{c,0}}{v_c} \right)^a \right] \quad (9)$$

with $\beta = 2.5$, $v_c(M)$ is the virial velocity for a halo of mass M , and the free parameters a , r_0 and $v_{c,0}$ are fixed by comparing the model predictions to the available observations.

The above model is mentioned only for completeness and we do not consider it further for fitting the data. The other two DLA-based models (Barnes & Haehnelt 2010, 2014) assign HI to dark matter haloes according to mass prescriptions, which enables comparison to the 21-cm based model. We hence consider these two DLA-based models for the remainder of the text. Both the models use the prescription for $M_{\text{HI}}(M)$ to be given by:

$$M_{\text{HI}}(M) = \alpha M f_{H,c} \exp \left[- \left(\frac{v_{c,0}}{v_c(M)} \right)^3 \right] \quad (10)$$

where α is the neutral fraction of HI in the halo (relative to cosmic), $f_{H,c} = (1 - Y_p) \Omega_b / \Omega_m$ is the cosmic hydrogen fraction and Y_p is the cosmological helium fraction by mass, and the parameter $v_{c,0}$ is a free parameter fixed by matching to the observations. The best-fit values are $v_{c,0} = 50$ km/s in Barnes & Haehnelt (2010) and $v_{c,0} = 90$ km/s in Barnes & Haehnelt (2014). In both models, the gas radial distribution profile is modelled as an altered NFW

4 Padmanabhan, Choudhury and Refregier

profile:

$$\rho_{\text{HI}}(r) = \frac{\rho_0 r_s^3}{(r + 0.75r_s)(r + r_s)^2} \quad (11)$$

where r_s is the scale radius, defined as $r_s = R_v(M)/c(M, z)$ with $R_v(M)$ being the virial radius:

$$R_v(M) = 46.1 \text{ kpc} \left(\frac{\Delta_v \Omega_m h^2}{24.4} \right)^{-1/3} \left(\frac{1+z}{3.3} \right)^{-1} \left(\frac{M}{10^{11} M_\odot} \right)^{1/3} \quad (12)$$

with $\Delta_v = 18\pi^2 + 82d - 39d^2$ and $d = \Omega_m(z) - 1 = \Omega_m(1+z)^3 / (\Omega_m(1+z)^3 + \Omega_\Lambda) - 1$ (Bryan & Norman 1998). The parameter c is the halo concentration approximated by:

$$c(M, z) = c_{\text{HI}} \left(\frac{M}{10^{11} M_\odot} \right)^{-0.109} \left(\frac{4}{1+z} \right) \quad (13)$$

where c_{HI} is the concentration parameter for the HI, which is analogous to the dark matter halo concentration $c_0 = 3.4$ in Macciò et al. (2007). Typically, one finds that c_{HI} is larger than c_0 . The normalization ρ_0 in Eq. (11) is determined by the condition that:

$$\int_0^{R_v(M)} 4\pi r^2 \rho_{\text{HI}}(r) dr = M_{\text{HI}}(M) \quad (14)$$

The best-fit value of the parameter c_{HI} is found to be $c_{\text{HI}} = 25$ in both DLA based models.

We now attempt to combine the above three prescriptions into similar functional forms. To do this, we introduce exponential lower and upper cutoffs in the 21-cm based mass prescription, of 30 and 200 km/s respectively:

$$M_{\text{HI}}(M) = \alpha f_{\text{H},c} M \exp \left[- \left(\frac{v_{c,0}}{v_c(M)} \right)^3 \right] \exp \left[- \left(\frac{v_c(M)}{v_{c,1}} \right)^3 \right] \quad (15)$$

where $v_{c,0} = 30$ km/s, $v_{c,1} = 200$ km/s, and α is an overall normalization parameter which denotes the fraction of HI in the halo relative to cosmic. The functional form adopted in Eq. (15) also applies to the two DLA based prescriptions, with $v_{c,1} = \infty^4$ and $v_{c,0} = 50$ km/s and 90 km/s, respectively. Hence, we may parametrize the three prescriptions by their cutoff velocities. These are plotted in Fig. 1.

The quantities α , c_{HI} , $v_{c,0}$ and $v_{c,1}$ have direct physical implications in the calculations of the relevant observables involved in estimating the 21-cm HI power spectrum. α provides the overall normalization (the HI fraction in the halo relative to cosmic) and c_{HI} describes the concentration of HI relative to the underlying dark matter distribution. These two parameters may be fixed by comparing to the observations of dN/dX and f_{HI} . The two cutoffs, $v_{c,0}$ and $v_{c,1}$ select the range in the mass function that contributes significantly to the bias b_{HI} (at low redshifts) or b_{DLA} (at higher redshifts). Note that in the absence of the cutoffs (i.e. if $M_{\text{HI}} \propto M$ for all M), we would have:

$$b_{\text{HI}}(z) = \frac{\int_0^\infty dM n(M, z) b(M, z) M}{\int_0^\infty dM n(M, z) M} = 1 \quad (16)$$

which follows from the results in Seljak (2000); Refregier & Teyssier (2002). Hence, the lower and upper cutoffs in the HI mass prescription are directly related to the calculated bias.

⁴ In practice, we may adopt a very high (~ 10000 km/s) upper cutoff for these models. The decline of the mass function at the high mass end provides a natural high mass cutoff to these prescriptions.

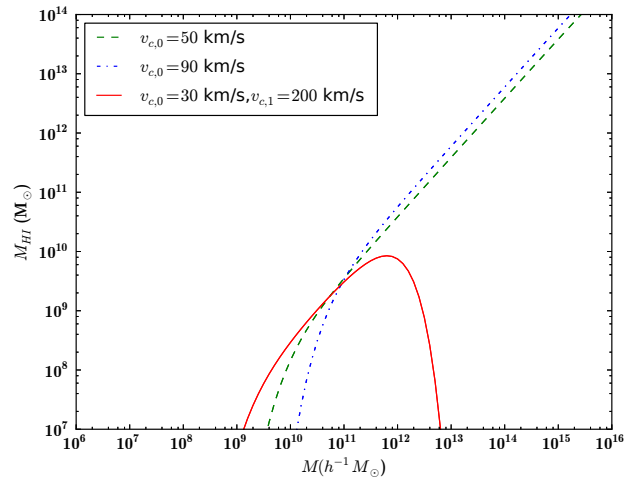


Figure 1. Prescriptions for the 21-cm based and the two DLA based models (plotted here at $z = 2.3$). The difference between the prescriptions arises from the range of mass values probed.

$v_{c,0} \backslash z$	0	1	1.5	2	2.3	3	4
90 km/s	0.11	0.13	0.2	0.25	0.34	0.4	1.0
50 km/s	0.09	0.13	0.2	0.21	0.22	0.3	0.5
30 km/s	0.15	0.15	0.3	0.3	0.3	0.3	0.48

Table 1. The values of α , the overall normalization relative to cosmic of neutral hydrogen in the three models under consideration, chosen for consistency with the observed values of the incidence rate dN/dX at redshifts 0 - 4, and the f_{HI} distribution, where available.

It can be seen from Fig. 1 that the 21-cm and DLA based models are very different with respect to the choice of host halo masses for assignment of neutral hydrogen. The results of simulations disfavour the assignment of HI gas to halos with virial velocities smaller than 30 km/s (or halo masses below $10^9 M_\odot$ at $z \sim 2.3$). Also, haloes of masses corresponding to virial velocities greater than 200 km/s ($M \sim 10^{12} M_\odot$ at $z \sim 2.3$) are not expected to host HI (Pontzen et al. 2008). We, therefore, attempt here to extend the 21-cm based prescription to also account for the available DLA observables.

We use the mass prescription Eq. (15) with the HI profile given by Eq. (11) to model the observables, for all three choices of cutoffs: (a) $v_{c,0} = 90$ km/s, $v_{c,1} = \infty$ (b) $v_{c,0} = 50$ km/s, $v_{c,1} = \infty$ and (c) $v_{c,0} = 30$ km/s, $v_{c,1} = 200$ km/s. At each redshift, we vary the parameters c_{HI} and α to match the observed column density distribution f_{HI} , where available, and the incidence rate of the DLAs, dN/dX . The quantities Ω_{HI} , b_{DLA} , $b_{\text{HI,gal}}$ and Ω_{DLA} then arise as predictions of the model. Note that the calculated values of the bias b_{HI} are fixed by the cutoffs considered in the prescription, and do not depend on c_{HI} and α . Hence, a different evolutionary scenario for α and c_{HI} would also lead to the same values of the calculated bias.

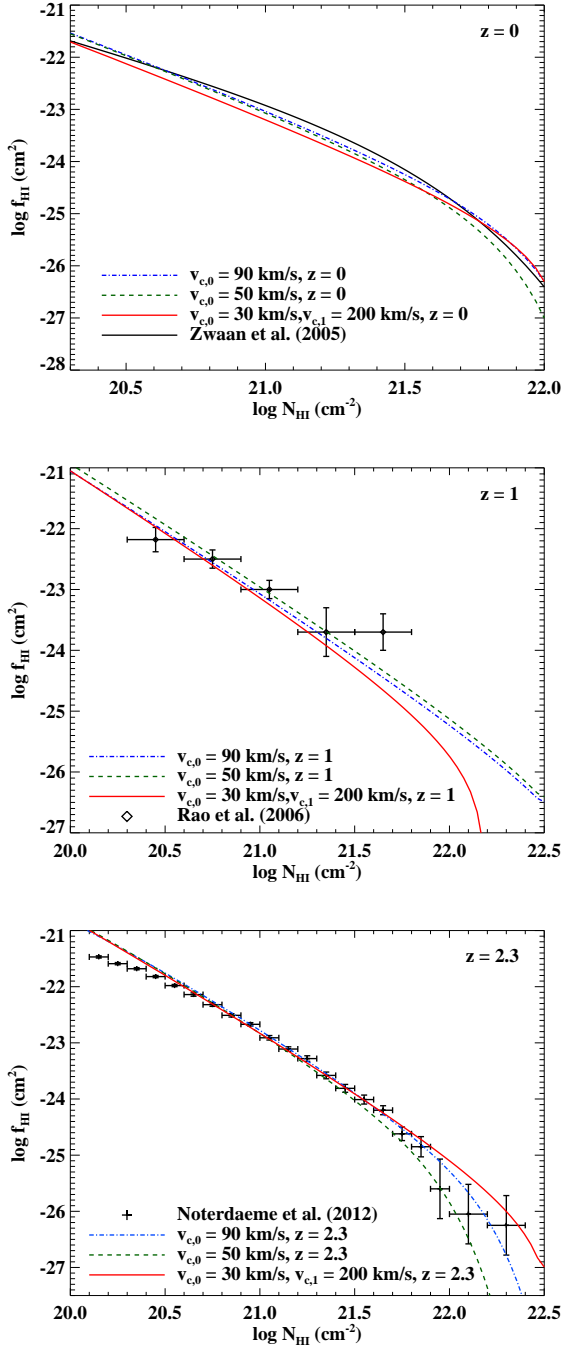


Figure 2. *Top panel:* The column density distribution f_{HI} for the three models, at redshift $z \sim 0$, together with the fitting function of Zwaan et al. (2005b). *Middle panel:* The f_{HI} at $z \sim 1$, with the data points from Rao, Turnshek & Nestor (2006). *Lower panel:* The f_{HI} at $z \sim 2.3$, with the data points from Noterdaeme et al. (2012). The models are labelled by their cutoff velocities.

4.1 Fitting the models to the observations

We now use the models and the available data to constrain the free parameters. In this work, we allow the parameters to vary independently at each redshift, thus making no assumptions *a priori* about how they evolve with redshift. This ensures that we exploit the maximum freedom available within the models to draw conclu-

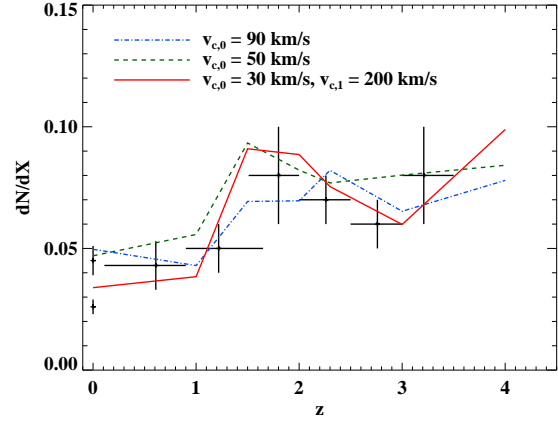


Figure 3. The DLA incidence dN/dX from the observations of Braun (2012); Zafar et al. (2013); Zwaan et al. (2005b); Rao, Turnshek & Nestor (2006) and fitted by the three models considered.

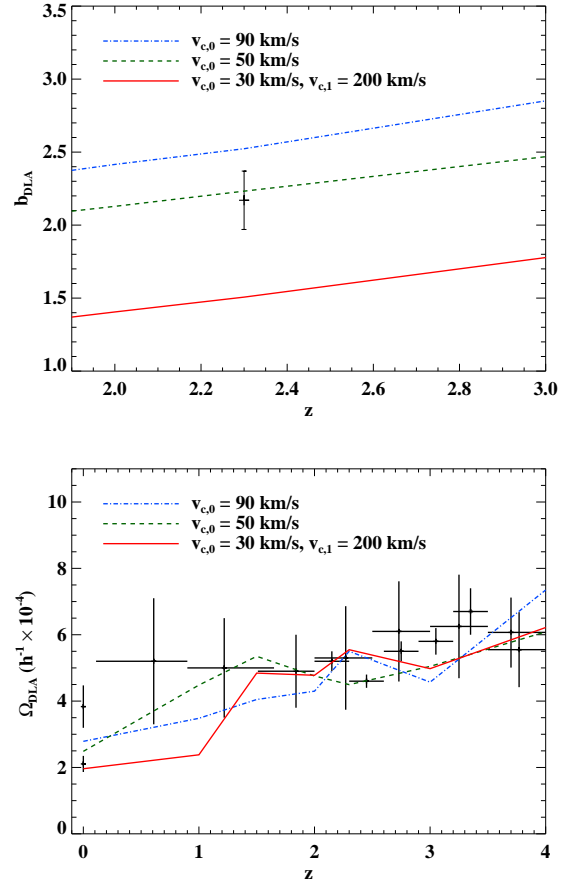


Figure 4. *Top panel:* The predicted values of b_{DLA} from the three models, and the data point from Font-Ribera et al. (2012). *Lower panel:* The values of Ω_{DLA} from the three models, along with the data points (Zwaan et al. 2005a; Braun 2012; Rao, Turnshek & Nestor 2006; Prochaska & Wolfe 2009; Noterdaeme et al. 2012; Zafar et al. 2013).

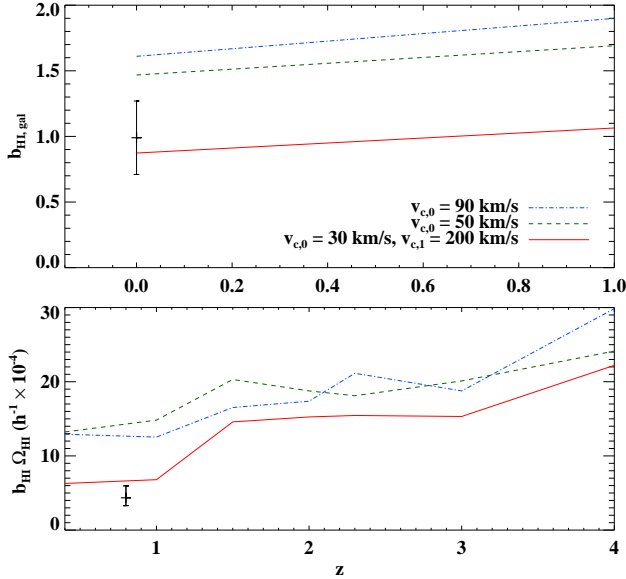


Figure 5. The low-redshift data, along with the model predictions. *Top panel:* The bias $b_{\text{HI,gal}}$ along with the $z \sim 0$ measurement (Martin et al. 2012). *Lower panel:* The product $\Omega_{\text{HI}} b_{\text{HI}}$ at all redshifts $z \sim 0 - 4$ as predicted by the models, along with the $z \sim 0.8$ measurement (Switzer et al. 2013).

sions which are robust. Since the available observations are not all at the same set of redshift values, we choose a representative set of redshifts (0, 1, 1.5, 2, 2.3, 3, 4) at which the model outputs are generated. At $z = 0$, $z = 1$, and 2.3, the parameters c_{HI} and α are fixed by the observed f_{HI} . The c_{HI} determines the overall "slope" of the curve, and α , the normalization, determines its height (this is discussed in detail in Barnes & Haehnelt (2010), see figure 7 of the paper) and hence both these parameters are constrained by the observed f_{HI} . The value of $c_{\text{HI}} = 25$ at $z \sim 2.3$ in both the DLA-based models (Barnes & Haehnelt 2010, 2014), and is found to be higher ($c_{\text{HI}} = 40$ and $c_{\text{HI}} = 100$ respectively) at $z = 0, 1$. For all the three redshifts, $c_{\text{HI}} = 60$ in the 21-cm based model. At $z = 1.5, 2, 3, 4$, where the observations of f_{HI} are not available, the parameters c_{HI} and α are chosen to match the observations of dN/dX and Ω_{DLA} . The remaining observables then arise as the model predictions. Thus, the model free parameters are fixed to simultaneously match the observations of f_{HI} (where available), Ω_{DLA} and dN/dX across redshifts 0-4. The values of α thus considered are indicated in Table 1, which indicate a trend of depleting HI gas towards lower redshifts.

The f_{HI} distributions are plotted in Figs. 2 along with the available observational data from Zwaan et al. (2005b, a fitting function), Rao, Turnshek & Nestor (2006, data points) and Noterdaeme et al. (2012, data points). The observed values of dN/dX (Zwaan et al. 2005b; Rao, Turnshek & Nestor 2006; Braun 2012; Zafar et al. 2013) are plotted in Fig. 3 and fitted by the three models.⁵

The predicted bias b_{DLA} (Font-Ribera et al. 2012) and neutral hydrogen density parameter Ω_{DLA} (Braun 2012; Rao, Turnshek & Nestor 2006; Prochaska & Wolfe 2009;

⁵ The fitted value of dN/dX at $z = 0$ is the average of the two measurements at this redshift, from Zwaan et al. (2005b) and Braun (2012).

Noterdaeme et al. 2012; Zafar et al. 2013) are plotted in Fig. 4 along with the data points.⁶ It can be seen that the the 21-cm based prescription is a poor match to the observed value of DLA bias at $z \sim 2.3$, while the DLA-based predictions are closer to the observed value.

The parameters Ω_{HI} and b_{HI} are then predicted by the models once the values of c_{HI} and α are fixed.⁷ The observation of b_{HI} (at $z \sim 0$) from the ALFALFA survey⁸ (Martin et al. 2012) is plotted in the top panel of Fig. 5 along with the predictions of the models. At $z \sim 0$, the bias $b_{\text{HI,gal}}$ measured by the ALFALFA survey is primarily sensitive to galaxies having HI masses above $10^6 M_{\odot}$. Accordingly, at $z = 0$, we have neglected the contributions of M_{HI} masses below $10^6 M_{\odot}$ while calculating the values of $b_{\text{HI,gal}}$ from the models.

The model predictions for the product $\Omega_{\text{HI}} b_{\text{HI}}$ at all redshifts $z \sim 0 - 4$, along with the intensity mapping measurement (Switzer et al. 2013) at $z \sim 0.8$ are plotted in the lower panel of Fig. 5. The model predictions at higher redshifts would be useful for comparing with observations in upcoming intensity mapping experiments.

The 21-cm based prescription ($v_{c,0} = 30$ km/s, $v_{c,1} = 200$ km/s) that we consider here, extended to account for the DLA observables, is consistent with the majority of the low-redshift observations. It also matches the DLA observables at higher redshifts except the high value of $b_{\text{DLA}} \sim 2.17$ at redshift 2.3 (the model leads to $b_{\text{DLA}} \sim 1.5$). The model also reasonably matches the constraint $\Omega_{\text{HI}} b_{\text{HI}}$ at $z \sim 0.8$ (Switzer et al. 2013) and the bias $b_{\text{HI,gal}}$ at low redshifts $z \sim 0$ (Martin et al. 2012) as shown in Fig. 5.

The DLA based prescriptions, on the other hand, lead to values of b_{HI} and $\Omega_{\text{HI}} b_{\text{HI}}$ which are higher than observed at $z \sim 0 - 1$. However, these prescriptions are consistent with the high value of b_{DLA} at $z \sim 2.3$.

5 DISCUSSION

As we have seen, two independent observational techniques are used to constrain the distribution and evolution of HI in the post-reionization universe — the DLA observations and the 21-cm based measurements. These two observational techniques have, in turn, been typically associated with their own theoretical and analytical prescriptions. While the two sets of analytical techniques have been applied separately to the corresponding observations in the existing literature, here we attempt to connect these approaches to take into account all the available data, in a common framework from both these sets of measurements simultaneously. This is particularly relevant because both these observational probes — DLAs as well as 21-cm based measurements — are sensitive to the high-column density neutral gas, and hence also important probes of large-scale structure formation.

⁶ The Zwaan et al. (2005a) measurement at $z = 0$ for atomic gas mass density has been corrected for by factor 0.81 for comparison to the measurements from DLAs, according to the results of Zwaan et al. (2005b).

⁷ The predicted value of Ω_{HI} is always found to be greater than Ω_{DLA} . This is consistent with expectations because the Ω_{DLA} contains contribution only from systems having $N_{\text{HI}} > 10^{20.3} \text{ cm}^{-2}$, while the Ω_{HI} measured from intensity mapping experiments contains contributions from the whole range of HI column densities.

⁸ Above $10 h^{-1}$ Mpc, the bias parameter becomes independent of scale. The ALFALFA data provide the bias parameter as a function of scale; here, we plot the mean bias and its associated error at all scales $\gtrsim 10 h^{-1}$ Mpc as measured by this survey.

In this paper, we have attempted to reconcile the 21-cm and the DLA based prescriptions to describe the characteristics of HI host haloes at various redshifts in the post-reionization universe. We have summarized the existing models for the 21-cm and the DLA based prescriptions for assigning HI to dark matter halos. We have modified and extended the existing 21-cm based model to account for the DLA observations, and also extended the DLA-based models to all redshifts 0-4. In each case, and at every redshift, we have calibrated the model free parameters by matching the available observations. Our main findings may be summarized as follows:

(i) A physically motivated, 21-cm based prescription ($v_{c,0} = 30$ km/s, $v_{c,1} = 200$ km/s), in combination with a halo profile for the distribution of HI, provides a good fit to the majority of the available data. It matches the observed low value of the HI bias at $z \sim 0$, and of the product $\Omega_{\text{HI}} b_{\text{HI}}$ at $z \sim 1$. The model is also consistent with the DLA observations of f_{HI} , Ω_{DLA} and dN/dX at $z \sim 0 - 4$. However, at $z \sim 2.3$, the model leads to a lower value of DLA bias b_{DLA} than is observed.

(ii) The two DLA-based models, having cutoffs of $v_{c,0} = 50$ and 90 km/s respectively, are consistent with the measurement of b_{DLA} at $z \sim 2.3$. The clustering measurement, therefore, requires the lower cutoff in the sampling of the halo mass function to be close to 50-90 km/s. It also favours the presence of a very high (or the absence of a) high mass cutoff. Both these factors suggest that the observed DLA bias at $z \sim 2.3$ is well reproduced if the neutral hydrogen in shallow potential wells is depleted, thus suggesting the possibility of very efficient stellar feedback (Barnes & Haehnelt 2014). However, it is difficult to reconcile models having such strong feedback with the low-redshift observations of HI bias and $\Omega_{\text{HI}} b_{\text{HI}}$.

(iii) This highlights a tension between the DLA bias and the 21-cm measurements, unless there is a significant change in the nature of HI-bearing systems across redshifts 0-3, i.e. from lower-mass haloes at low redshifts to more massive haloes at higher redshifts. It is important to note that this result holds irrespective of how the free parameters α and c_{HI} evolve with time, and thus directly constrains the maximum and minimum masses of the haloes under consideration.

(iv) This also has implications for the measured 21-cm intensity fluctuation power spectrum. Taken together, the observed bias measurements at $z \sim 0$ and $z \sim 2.3$ suggest an almost factor of two evolution in the bias between redshifts 0-3, which alone implies a factor 4 evolution in the measured power spectrum of intensity fluctuations.

These findings can be related to other lines of investigation into the nature of high-redshift DLA hosts. The results of the 21-cm based model lead to a DLA bias ($b_{\text{DLA}} \sim 1.5$ at redshift $z \sim 2.3$) which is lower than the observed value. The model suggests that DLAs are hosted by faint dwarf galaxies at high redshift ($z \sim 2.3$). This finding is consistent with the observed lack of nearby high-luminosity galaxies at high redshifts (Cooke, Pettini & Jorgenson 2015). It has been suggested (Fumagalli et al. 2015) that the DLAs are hosted by faint dwarf galaxies which are either isolated or clustered with more massive galaxies. The observed high value of bias b_{DLA} may be explained if the DLAs arise from dwarf galaxies which are satellites of massive Lyman-break galaxies (Font-Ribera et al. 2012). However, the lack of bright Lyman-break galaxies in the vicinity of DLAs (Fumagalli et al. 2015) suggests that DLAs may be isolated dwarf Lyman-break galaxies, which would lead to a much

lower bias than observed at $z \sim 2.3$. The low star formation rates ($0.09 - 0.27 M_{\odot} \text{ yr}^{-1}$; Fumagalli et al. 2015) associated with these systems typically correspond to host haloes of masses $\lesssim 10^{11} M_{\odot}$ at $z \sim 2$ (e.g., Behroozi, Wechsler & Conroy 2013). The results of cosmological simulations also support this view since DLAs arise in host haloes of masses $10^9 - 10^{11} M_{\odot}$ at redshift $z \sim 3$ (Pontzen et al. 2008; Tescari et al. 2009; Fumagalli et al. 2011; Cen 2012; van de Voort et al. 2012; Bird et al. 2013; Rahmati & Schaye 2014).⁹ It is also found in simulations (Davé et al. 2013) that at these redshifts, only half the cosmic HI resides in $M_{\text{HI}} > 10^9 M_{\odot}$ systems, with a very small fraction in $M_{\text{HI}} > 10^{10} M_{\odot}$ systems. Hence, the 21-cm based model, while inconsistent with the high-redshift bias measurement, is indeed consistent with the recent results of imaging and other surveys of high-redshift DLAs.

In future work, it would be useful to compare our analytical results with the semianalytical and simulation studies (e.g., Bird et al. 2013; Rahmati & Schaye 2014; Cen 2012; Tescari et al. 2009). This would, in turn, also have important consequences for determining the 21-cm intensity fluctuation power spectrum, and hence better understanding the distribution and evolution of neutral hydrogen in the post-reionization universe.

ACKNOWLEDGEMENTS

HP acknowledges support from the SPM research grant of the Council of Scientific and Industrial Research (CSIR), India. We thank Varun Bhalerao, Jayaram Chengalur, Romeel Davé, Nissim Kanekar, Roy Maartens, Sebastian Seehars, R. Srianand, Kaustubh Vaghmare and Francisco Villaescusa-Navarro for useful discussions and comments on the manuscript. We thank the anonymous referee for useful comments that improved the content and presentation of the paper.

REFERENCES

- Bagla J. S., Khandai N., Datta K. K., 2010, MNRAS, 407, 567
 Barnes D. G. et al., 2001, MNRAS, 322, 486
 Barnes L. A., Haehnelt M. G., 2009, MNRAS, 397, 511
 Barnes L. A., Haehnelt M. G., 2010, MNRAS, 403, 870
 Barnes L. A., Haehnelt M. G., 2014, MNRAS, 440, 2313
 Behroozi P. S., Wechsler R. H., Conroy C., 2013, ApJ, 770, 57
 Bird S., Vogelsberger M., Haehnelt M., Sijacki D., Genel S., Torrey P., Springel V., Hernquist L., 2014, MNRAS, 445, 2313
 Bird S., Vogelsberger M., Sijacki D., Zaldarriaga M., Springel V., Hernquist L., 2013, MNRAS, 429, 3341
 Bouché N., Murphy M. T., Kacprzak G. G., Péroux C., Contini T., Martin C. L., Dessauges-Zavadsky M., 2013, Science, 341, 50
 Braun R., 2012, ApJ, 749, 87
 Bryan G. L., Norman M. L., 1998, ApJ, 495, 80
 Bull P., Ferreira P. G., Patel P., Santos M. G., 2015, ApJ, 803, 21
 Catinella B. et al., 2010, MNRAS, 403, 683
 Cen R., 2012, ApJ, 748, 121
 Chang T.-C., Pen U.-L., Bandura K., Peterson J. B., 2010, Nature, 466, 463

⁹ The incidence rate for the DLAs as a function of host halo mass, also shows a peak around host halo masses of $M \sim 10^{9.5} - 10^{12} M_{\odot}$ at $z \sim 2.3$ in the 21-cm based prescription, consistent with previous findings of Barnes & Haehnelt (2010) which point to DLAs being hosted by dark matter haloes with virial velocities in the range 35-230 km/s.

- Cooke R. J., Pettini M., Jorgenson R. A., 2015, *ApJ*, 800, 12
- Davé R., Katz N., Oppenheimer B. D., Kollmeier J. A., Weinberg D. H., 2013, *MNRAS*, 434, 2645
- Delhaize J., Meyer M. J., Staveley-Smith L., Boyle B. J., 2013, *MNRAS*, 433, 1398
- Font-Ribera A. et al., 2012, *JCAP*, 11, 59
- Freudling W. et al., 2011, *ApJ*, 727, 40
- Fumagalli M., O'Meara J. M., Prochaska J. X., Kanekar N., Wolfe A. M., 2014, *MNRAS*, 444, 1282
- Fumagalli M., O'Meara J. M., Prochaska J. X., Rafelski M., Kanekar N., 2015, *MNRAS*, 446, 3178
- Fumagalli M., Prochaska J. X., Kasen D., Dekel A., Ceverino D., Primack J. R., 2011, *MNRAS*, 418, 1796
- Fynbo J. P. U. et al., 2013, *MNRAS*, 436, 361
- Fynbo J. P. U. et al., 2010, *MNRAS*, 408, 2128
- Fynbo J. P. U. et al., 2011, *MNRAS*, 413, 2481
- Gardner J. P., Katz N., Hernquist L., Weinberg D. H., 1997, *ApJ*, 484, 31
- Giovanelli R. et al., 2005, *AJ*, 130, 2598
- Guha Sarkar T., Mitra S., Majumdar S., Choudhury T. R., 2012, *MNRAS*, 421, 3570
- Hong S., Katz N., Davé R., Fardal M., Kereš D., Oppenheimer B. D., 2010, *arXiv:1008.4242*
- Jaffé Y. L., Poggianti B. M., Verheijen M. A. W., Deshev B. Z., van Gorkom J. H., 2012, *ApJ*, 756, L28
- Jonas J. L., 2009, *IEEE Proceedings*, 97, 1522
- Lah P. et al., 2007, *MNRAS*, 376, 1357
- Lah P. et al., 2009, *MNRAS*, 399, 1447
- Lang R. H. et al., 2003, *VizieR Online Data Catalog*, 734, 20738
- Lanzetta K. M., Wolfe A. M., Turnshek D. A., Lu L., McMahon R. G., Hazard C., 1991, *ApJS*, 77, 1
- Macciò A. V., Dutton A. A., van den Bosch F. C., Moore B., Potter D., Stadel J., 2007, *MNRAS*, 378, 55
- Martin A. M., Giovanelli R., Haynes M. P., Guzzo L., 2012, *ApJ*, 750, 38
- Martin A. M., Papastergis E., Giovanelli R., Haynes M. P., Springob C. M., Stierwalt S., 2010, *ApJ*, 723, 1359
- Masui K. W. et al., 2013, *ApJ*, 763, L20
- Meyer M. J. et al., 2004, *MNRAS*, 350, 1195
- Nagamine K., Wolfe A. M., Hernquist L., Springel V., 2007, *ApJ*, 660, 945
- Noterdaeme P. et al., 2012, *A&A*, 547, L1
- Noterdaeme P., Petitjean P., Ledoux C., Srianand R., 2009, *A&A*, 505, 1087
- Olive K. A., Skillman E. D., 2004, *ApJ*, 617, 29
- Padmanabhan H., Choudhury T. R., Refregier A., 2015, *MNRAS*, 447, 3745
- Planck Collaboration et al., 2013, *arXiv:1303.5076*
- Pontzen A. et al., 2008, *MNRAS*, 390, 1349
- Prochaska J. X., Herbert-Fort S., Wolfe A. M., 2005, *ApJ*, 635, 123
- Prochaska J. X., Wolfe A. M., 2009, *ApJ*, 696, 1543
- Rafelski M., Neeleman M., Fumagalli M., Wolfe A. M., Prochaska J. X., 2014, *ApJ*, 782, L29
- Rahmati A., Schaye J., 2014, *MNRAS*, 438, 529
- Rao S. M., Turnshek D. A., Nestor D. B., 2006, *ApJ*, 636, 610
- Refregier A., Teyssier R., 2002, *Phys.Rev.D*, 66, 043002
- Rhee J., Zwaan M. A., Briggs F. H., Chengalur J. N., Lah P., Oosterloo T., Hulst T. v. d., 2013, *MNRAS*, 435, 2693
- Santos M., Alonso D., Bull P., Silva M. B., Yahya S., 2015, *Advancing Astrophysics with the Square Kilometre Array (AASKA14)*, 21
- Scoccimarro R., Sheth R. K., Hui L., Jain B., 2001, *ApJ*, 546, 20
- Seljak U., 2000, *MNRAS*, 318, 203
- Sheth R. K., Tormen G., 2002, *MNRAS*, 329, 61
- Storrie-Lombardi L. J., Wolfe A. M., 2000, *ApJ*, 543, 552
- Swarup G., Ananthkrishnan S., Kapahi V. K., Rao A. P., Subrahmanya C. R., Kulkarni V. K., 1991, *Current Science*, Vol. 60, NO.2/JAN25, P. 95, 1991, 60, 95
- Switzer E. R. et al., 2013, *MNRAS*, 434, L46
- Tescari E., Viel M., Tornatore L., Borgani S., 2009, *MNRAS*, 397, 411
- van de Voort F., Schaye J., Altay G., Theuns T., 2012, *MNRAS*, 421, 2809
- Villaescusa-Navarro F., Viel M., Datta K. K., Choudhury T. R., 2014, *arXiv:1405.6713*
- Wolfe A. M., Turnshek D. A., Smith H. E., Cohen R. D., 1986, *ApJS*, 61, 249
- Zafar T., Péroux C., Popping A., Milliard B., Deharveng J.-M., Frank S., 2013, *A&A*, 556, A141
- Zwaan M. A., Meyer M. J., Staveley-Smith L., Webster R. L., 2005a, *MNRAS*, 359, L30
- Zwaan M. A., van der Hulst J. M., Briggs F. H., Verheijen M. A. W., Ryan-Weber E. V., 2005b, *MNRAS*, 364, 1467